The carbon and hydrogen contents in ALD-grown ZnO films define a narrow ALD temperature window

B. Xia, J.J. Ganem, E. Briand, S. Steydli, H. Tancrez, Ian Vickridge

The carbon and hydrogen contents in ALD-grown ZnO films define a narrow ALD temperature window

B. Xia [1], J.J. Ganem [1], E. Briand[1], S. Steydli [1], H. Tancrez [1], I. Vickridge [1]
SAFIR, Institut de NanoSciences de Paris, UMR7588 du CNRS et Sorbonne Université - Paris (France), E-mail: bingbing.xia@insp.jussieu.fr (Bingbing XIA).

Abstract

Zinc oxide thin films grown by atomic layer deposition have been subject to great attention over the past few years. In this work, we study ZnO films grown on Si substrates by atomic layer deposition with di-ethyl zinc (DEZ) as metal precursor and H_2O or D_2O water vapour as oxidant. Film composition as a function of growth temperature is studied by Ion Beam Analysis (IBA) using Rutherford Backscattering Spectrometry (RBS) to determine Zn areal density; Nuclear Reaction Analysis (NRA) for C and O areal density, and Elastic Recoil Detection Analysis (ERDA) for hydrogen areal density. The Zn/O ratio is close to 1 within a broad ALD window consistent with previous studies, however the carbon content varies substantially within this window and is minimum only within a much narrower temperature range.

Key words: Atomic Layer Deposition (ALD), ZnO thin films, Ion beam analysis (IBA).

1. Introduction

Zinc oxide film as a semiconductor material with low production cost has attracted great attention in recent years, in particular due to its wide and direct band gap of 3.37 eV, and a high exciton binding energy of 60 meV that allows bright room temperature emission. Applications of thin-film ZnO have been found across numerous fields, such as supercapacitors, sensors and solar cells [1-4]. ZnO films are typically grown by Atomic Layer Deposition (ALD) [5, 6], Chemical Vapour Deposition (CVD) [7-9], Pulsed Laser Deposition (PLD) [10-12] and sol-gel methods [13, 14].

The requirements for reducing dimensions and increasing control in many applications, especially in microelectronics, have led to a strong interest in depositing ZnO films by ALD because of its self-limiting and highly conformal growth [15]. The composition, structure and growth mechanisms of ALD ZnO films have been studied by ellipsometry, transmission electron microscopy (TEM), and X-ray reflectivity (XRR) [16-19] amongst others. These observations, together with theoretical studies using density functional theory (DFT), molecular dynamics simulations and monte carlo methods have also yielded significant insight into the underlying reaction kinetics and growth modes of this ALD process [20-22]. The general characteristics of the surface chemistry at different temperatures, for various precursor pulse durations and pressures and as a function of the number of ALD cycles have been carefully presented in the previous works. The temperature window for nearly constant Growth Per Cycle (GPC), which is the significant parameter guiding ALD film preparation, has also been explored on different substrates. However, most of these studies defined

the ALD window as that where the growth rate was independent of deposition temperature, but paid little attention to the actual chemical composition of the films. The ALD window defined in this way was found to be of wide range and extending down to quite low temperatures. For example, S.-Y. Pung et.al. used di-ethyl zinc (DEZ) and water as precursors to deposit ZnO films on Si(100) and determined that the ZnO ALD window ranged from 125 to 150℃ [23]. S. Jeon et.al. presented the ALD window of ZnO films on Si(100) as ranging from 70 to 200℃ with the same precursors [24]. Kwon et.al. defined a higher ALD window for ZnO with temperature ranging from 150 to 200℃ [25], whilst Tapily et.al. and Illiberi et.al. found ALD windows for ZnO films from 100-160℃ and 110-160℃, respectively [26, 27]. Moataz Bellah et. al. give a much wider ALD window with temperature from 100-250℃ [28]. These works have made important contributions to the development of ZnO films grown by ALD, offering much insight into the growth mechanisms and highlighting the great potential application of ZnO films. However, the wide range and diversity of the observed ALD windows suggests that growth rate alone may not be sufficient to establish the best ALD growth conditions for ZnO.

Investigation of the impurities near to the surface as well as their depth distribution are extremely important for film application. However, few reports give quantified analysis of the impurity distribution from a few atomic layers to nano or deeper layer in ZnO film. ToF-SIMS measurements by P. Boryło et. al. [29], in which a 30 keV Bi^+ beam was used to generate H^+ and $ZnOH^+$ secondary ions gave some indication of the presence of hydrogen in ALD grown ZnO films, however the signal to noise ratio is rather modest and no quantitative conclusions are drawn. Aleksandra Seweryn et.al reported the contents of hydrogen and carbon in the films were determined with use of secondary ion mass spectroscopy (SIMS)[30]. They carefully investigate the carbon and hydrogen contents in the ZnO films even for samples deposited at different temperatures which give us some intuitive results. They are, however, short of distinguishing the source of hydrogen and giving the quantified analysis for H and D atoms, respectively. Table 1 shows a literature list of reported impurities and GPC for the ALD grown ZnO films from several precursors and different oxidants. Except to the mentioned above, there is few quantitative measurements of impurities distribution in ZnO films.

Table 1. the literature overview of the impurity level and GPC for ALD grown ZnO films from different ALD system, metal precursors and oxidants. Me = CH_3, Et = C_2H_5, - = not measured, XPS = X-ray photoelectron spectroscopy, TOF-ERDA = Time-of-Flight Elastic Recoil Detection Analysis, SIMS= Secondary ion mass spectrometry, T-ALD = thermal ALD, P-ALD = plasma-assistant ALD, QL= qualitative.

Precursor	oxidant	Tem. (℃)	GPC (Å)	C (%)	H (%)	Method	Type	Ref.
DEtZn	H_2O	100-250	-	-	1-3	SIMS	T-ALD	[31]
DEtZn	H_2O	100-270	0.5-1.3	QL	QL	SIMS	T-ALD	[32]
DMeZn	H_2O	100-240	0.5-1.0	QL	QL	SIMS	T-ALD	[32]

DEtZn	H_2O	130-200	1.3-1.5	QL	QL	SIMS	T-ALD	[33]
DEtZn	O_2	150	-	15-25	-	XPS	P-ALD	[34]
DEtZn	O_2	100	~2.0	QL	QL	SIMS	P-ALD	[35]
DEtZn	O_2	100, 300	-	QL	QL	SIMS	P-ALD	[36]
DEtZn	H_2O	100-350	0.5-1.8	QL	QL	SIMS	T-ALD	[29]
DEtZn	H_2O	70, 100	0.4-0.9	0.11-0.13	3.2-5.3	TOF-ERDA	T-ALD	[37]
DEtZn	O_3	100	~0.5	~16	~2.1	TOF-ERDA	T-ALD	[37]
DEtZn	H_2O	60-200	0.8-2	-	QL	Cal	T-ALD	[38]
DEtZn	H_2O	50-250	0.7-1.8	0-0.3	0.4-4.8	SIMS	T-ALD	[30]
DEtZn	O_3	50-250	0.4-0.7	0.2-5.3	0.3-14.5	SIMS	T-ALD	[30]
DEtZn	H_2O	100-250	1.2-2	QL	-	XPS	T-ALD	[39]
DEtZn	O_2	50-200	0.4-0.6	2-12	6-22	TOF-ERDA	P-ALD	[40]
DEtZn	H_2O	40-120	0.8-2.4	0.3-1.1	2-11	TOF-ERDA	T-ALD	[41]
DEtZn	H_2O	-	-	2.1-8.5	-	XPS	T-ALD	[42]

In this work, we systematically explore the impurity content and in particular the carbon and hydrogen areal density especially at low deposition temperature, since the presence of these elements could be indicators of incomplete precursor reactions. The different pulse time and purge time are selected to investigate the impurities level in the film. ZnO film densities grown at different temperature are seriously give considering the H and C impurities influence. In an attempt to identify the origin of the hydrogen that was found in the films, some films were grown using D_2O.

2. Materials and methods

The ZnO thin films were grown on Si (100), cleaned with acetone and ethanol, by atomic layer deposition in the growth chamber described in NIIMB[43] using DEZ and water. The precursors were transported to the growth chamber with N_2 gas, and a long N_2 purge time of 30s was used in order to prevent precursors mixing during deposition. DEZ was supplied in 15ms pulses, whilst the water pulse length ranged from 15ms to 100ms. The surface deposition temperature was controlled from 100℃ to 300℃ and the number of ALD cycles was varied from 5 to 60. The film deposition process is presented schematically in Fig.1a. Growth of films with isotopically enriched water was achieved simply by replacing the water feed bottle by a new one with a few ml of $D_2{}^{18}O$. This precursor is expensive, however the amount of water used for film growth is sufficiently small that many hundreds of films can be grown from just a ml or two of water.

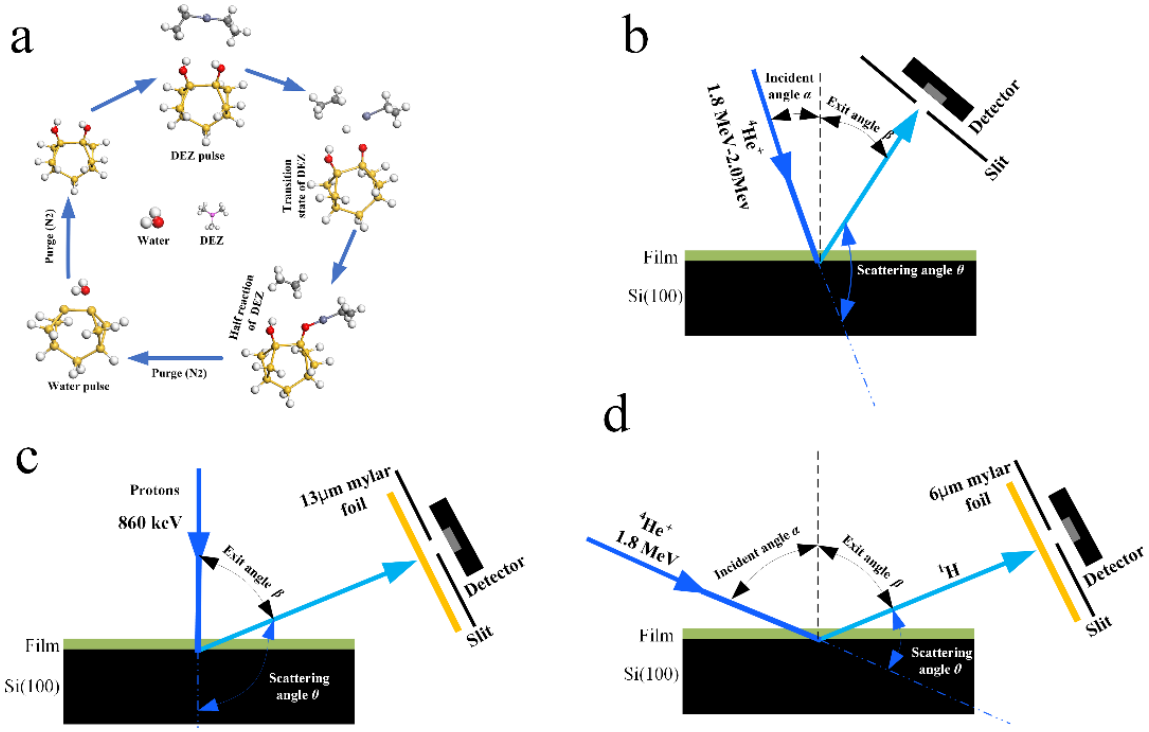

Fig.1. Methods. a: The deposition process of ZnO films. b, c, d: the detector geometry of RBS, NRA and ERDA, Incident angle α, exit angle β and scattering angle θ.

Ion Beam Analysis (IBA) was performed on the SAFIR platform at Sorbonne Université. Rutherford Backscattering Spectrometry (RBS) employed 20-100 nA $^4He^+$ beams of 1.5-2.1 MeV, in a 1mm diameter beamspot, with particle detection at 165° scattering angle (Fig. 1b). The detector solid angle was calibrated with 3% uncertainty using a Bi-implanted reference sample [44, 45]. Only the Zn areal density [Zn] was deduced from the RBS spectra. Nuclear Reaction Analysis (NRA) (Fig. 1c) was used to determine the ^{16}O and the ^{12}C areal densities [^{16}O] and [^{12}C] via the $^{16}O(d,p_1)^{17}O$ and $^{12}C(d,p_0)^{13}C$ nuclear reactions respectively, with respect to a thermal SiO_2 film, with [^{16}O]=625 ± 5×10^{15}atoms/cm^2 as deduced from the film thickness and density determined by ellipsometry[46]. An 860 keV deuteron beam of 85 nA in a 2mm beamspot was used, and the protons produced by the nuclear reactions were detected at 150° in a 300mm^2 detector behind a 13μm mylar foil which stopped the high flux of elastically scattered deuterons from saturating the detector. The oxygen reference also serves as a reference for the carbon areal density [^{12}C], since the cross sections and their ratio are known [47]. We can write:

$$[^{12}C] = \frac{Y_C}{Y_O}\frac{Q_O}{Q_C}\frac{\sigma_O}{\sigma_C}[^{16}O], \quad (1)$$

where Y_O and Y_C are the yields of protons from $^{16}O(d,p_1)^{17}O$ obtained on the reference sample and of protons from $^{12}C(d,p_0)^{13}C$ obtained from the films, respectively; [C] and [O] are the ^{12}C areal

density in the ZnO films and the ^{16}O areal density of the reference sample; σ_C and σ_O are the corresponding nuclear reaction cross sections, and Qo and Qc are the total incident beam charges for the film and reference measurements.

Hydrogen and deuterium areal densities were determined by Elastic Recoil Detection Analysis (ERDA) (Fig. 1d) with an 80 nA 1.8 or 2.0 MeV $^4He^+$ incident beam, and recoil detection at 30° scattering angle in a collimated detector behind a 9.15 μm mylar film. Spin-coated polyethylene films with the hydrogen $(C_2H_4)_n$ or deuterium $(C_2D_4)_n$ content deduced from the C content measured by NRA, were used as H and D references[48, 49].

Atomic force microscope (AFM) measurements of surface morphology were carried out with a Bruker Extended D3100 AFM. The crystallinity and phase composition of films were determined by X-ray diffraction (XRD). A PaNalytical X'Pert MRD 4 circles diffractometer was used, with a 1.54056 Å X-ray source, a hybrid two-bounce Ge (220) monochromator, and a Pixel detector. Film density was deduced from the film physical thickness and mass thickness obtained from spectroscopic ellipsometry (SE) and RBS, respectively. The SE measurements were made with a FS-1 Multi-Wavelength Ellipsometer system in the wavelength range of 465-635 nm at an angle of incidence of 65°.

3. Results and discussion

3.1 The film growth rate

Fig.2a shows the growth per cycle measured by RBS as a function of the deposition temperature with a given DEZ precursor time of 15ms and H_2O pulse time of 100ms for 40 cycles. [Zn]/cycle ranged from 1.5×10^{15} atoms/cm^2 to 6×10^{15} atoms/cm^2. The lowest [Zn]/cycle occurs at 100°C. This is most likely due to insufficient thermal activation of the reaction between the DEZ precursor and -OH groups on the Si surface as shown by M. Rueter [50]. [Zn]/cycle increases with temperature and is a maximum in the ALD window, before decreasing again as the temperatures rises above 175°C. This is consistent with the proposal by M. Rueter that the DEZ may be decomposed into Zn and ethyl fragments on the growth surface at higher temperatures, inhibiting growth on the substrate [50]. Water desorption at higher temperature also inhibits the formation of -OH groups, giving an additional cause for the lower growth rate. The stable [Zn]/cycle in the temperature window between 150 and 175°C suggests that self-limiting ALD growth of ZnO films has been obtained, as has been observed for very similar ALD windows in previous works [17-19]. [O]/cycle shown in Fig 2b presents practically the same growth trend as that of Zn, with a maximum of about $6x10^{15}$ atoms/cm^2 per cycle between 150°C and175°C as for Zn. [Zn]/cycle and [O]/cycle are very similar, which demonstrates that a reasonable atomic ratio of Zn to O will be obtained. Typical RBS and NRA spectra of ZnO films at 300°C, 175°C, 140°C, 125°C are presented in the Fig.2c and Fig.2d, respectively (details for other deposition temperatures are presented in supporting information

Fig.S1). From the RBS and NRA determinations of [Zn] and [^{16}O], we can divide the reaction states of DEZ and -OH into three regimes according to the deposition temperature: (1) 100-150℃: incomplete reaction; (2) 150 - 175℃: completed reaction (ALD window); (3) above 175℃: decomposition reaction.

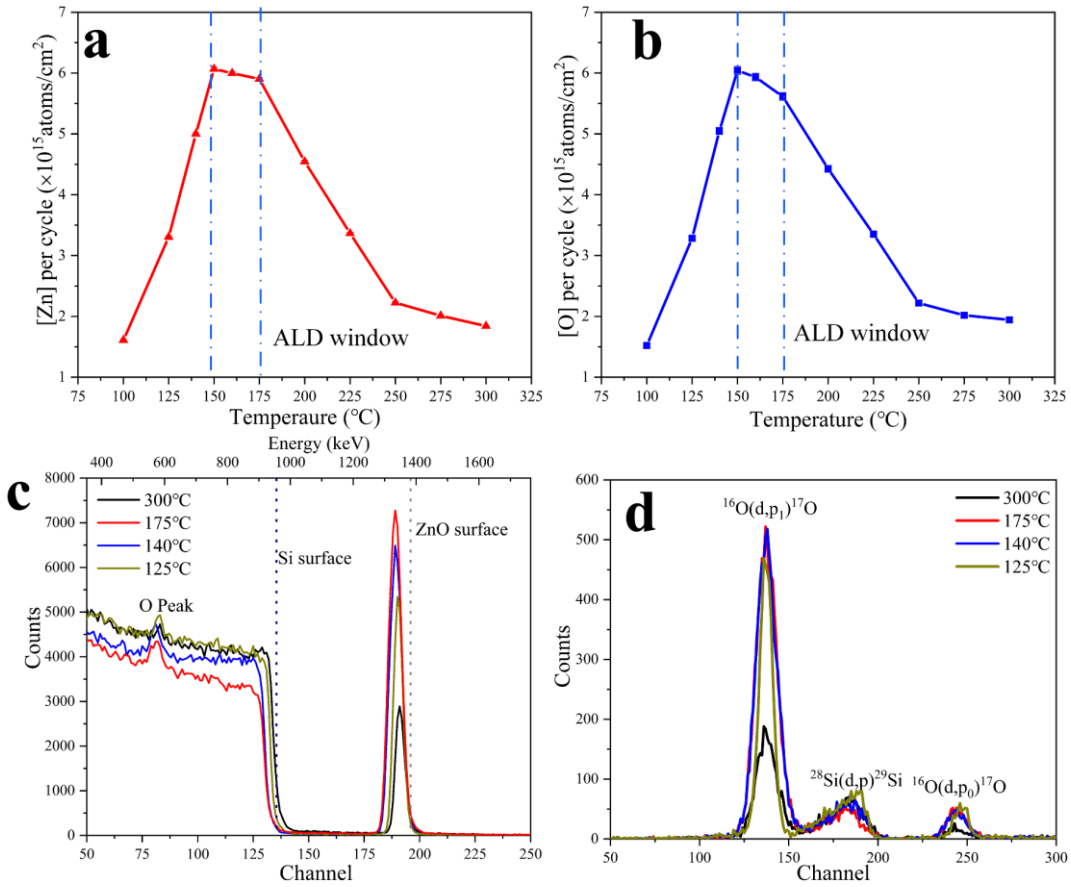

Fig.2. a: Zn areal density [Zn] for 40 ALD cycles as a function of the deposition temperature. b: The variation in O areal density [O] of ALD deposition as a function of the deposition temperature. c: Typical RBS spectra of ZnO films grown at different temperature. d: Typical NRA spectra of ZnO films grown at different temperature.

3.2 The carbon content of the ZnO films

Fig.3 shows [C]/cycle obtained from equation 1. [C]/cycle is much higher at temperatures either side of the ALD window, and falls again as temperatures rise above about 240°C. The highest [C]/cycle is found to be 0.68×10^{15} atoms/cm^2, for a deposition temperature of 100°C where [Zn]/cycle and [O]/cycle were about 1.5×10^{15} at/cm^2. This corresponds to about 15 atom% of carbon in the film, and suggests that the DEZ molecule couldn't completely react with -OH on the surface even if the surface has enough -OH. Hence, a fraction of the DEZ molecules just adsorb on the surface, leading to the high content of carbon in the films. Previous study also showed that adsorbed DEZ molecules on the Si (100) surface could dissociate below 127°C, producing Zinc metal and

adsorbed groups[51]. Such adsorbed fragments in the films could also cause the higher [C]/cycle. The excess ratio 1.06 of Zn to O at lower temperature also illustrates the dissociation of DEZ and incomplete reaction with -OH on the Si (100) surface (Fig.8a).

With increasing temperature, the [C]/cycle decreases to its lowest level of about 1.5×10^{15} at/cm^2 corresponding to about 1 atom% at 160°C, within the ALD window. The DEZ molecules interact with the -OH on the surface and form adsorbed ZnO islands or clusters[52]. The ethyl groups can react with hydrogen released from -OH groups, forming ethane which is flushed away during the N_2 purge.

However, the [C]/cycle in the films increases again between 175 and 225°C. We surmise here that some of the adsorbed DEZ molecules decomposed before bridging with -OH on the Si (100) surface. This would lead to the ethylene fragments bonding with the surface -OH and occupying the reactive site for -Zn-CH_2-CH_3 or -Zn-OH formation. Previous study showed that DEZ molecules heated to about 177°C decompose completely to form hydrocarbon molecules and zinc atoms [2]. This is consistent with our results and adsorption of hydrocarbon on the growth surface is probably the source of C content at higher temperature.

Furthermore, at higher temperature, although the chamber is not deliberately heated, thermal radiation from the substrate still increases the temperature of the elements surrounding the substrate plate, including the chamber walls, where the DEZ may be decomposed into Zn and ethyl fragments before coming into contact with the substrate, reducing the availability of DEZ for reaction with the sample growth surface.

In summary, we propose that deposition temperatures below the ALD window will cause higher carbon areal density in the films due to incomplete reaction, while for deposition temperatures above the ALD window increased carbon areal density is the result of the decomposition reaction of DEZ molecules on contact with the growth surface. Above about 225°C, DEZ decomposes into atomic Zn and weakly reactive organic fragments before coming into contact with the growth surface, resulting in lower residual carbon areal density in the films.

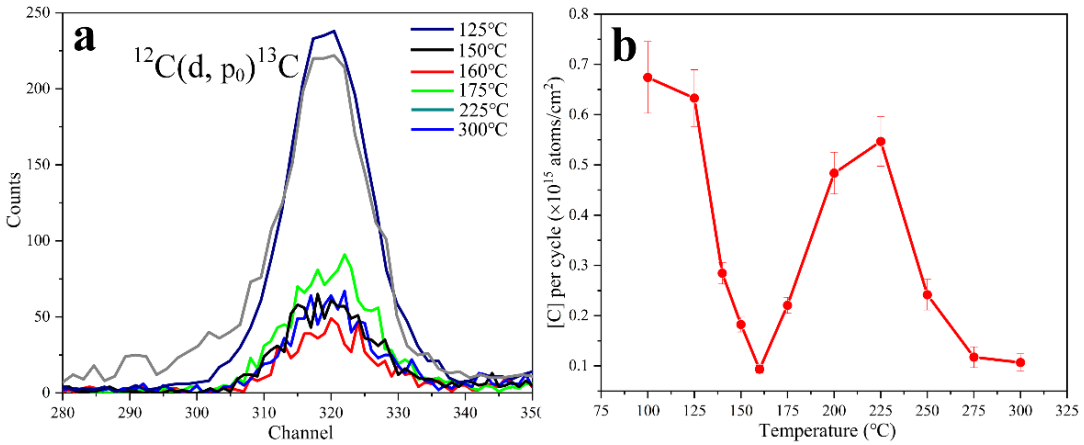

Fig.3. a: Carbon analysis obtained from the NRA spectra (Fig.1); b: Carbon areal density per cycle in ZnO film.

3.3 Hydrogen content of the ZnO films

As it is well known that hydrogen is also involved in the ALD process [20], we employed elastic recoil detection analysis (ERDA) to determine the hydrogen depth distribution in the ZnO films. Fig.4 shows ERDA spectra from film growth with deposition temperature, and at the lower and higher limits of the ALD temperature window. Fig.5 shows the hydrogen concentration depth profiles deduced by simulation with SimNRA [49, 53]. Spectra and profiles from intermediate growth temperature are shown in supplementary information (Figure S2 and S3). The recoil cross-sections for the H and D are non-Rutherford. The cross-section data of SigmaCalc[53] and Quillet, V[49] for $H(\alpha,p)^4He$ and $^2H(\alpha,d)^4He$ were used for the simulation, respectively. For all fitting, a contamination layer of 20×10^{15} at/cm^2 of CH_x ($H=3.3\times10^{15}$ at/cm^2) was assumed for the surface contamination. This is consistent with what we often observe in ERDA measurements of many types of sample, and the conclusions drawn here are not very sensistive to variations of a factor of two in this assumed layer.

Fig.4a shows the ERDA analysis for film deposited at 100℃. The channels from 300 to 275, represent the hydrogen in the ZnO films, which could be due either to remaining unreacted -OH groups or to adsorbed DEZ molecules that have not reacted with the water vapor. This observation and the high level of carbon at this temperature, are consistent with adsorption of DEZ molecules which have not reacted completely. According to the DFT calculation by Weckman, DEZ molecules form a pre-adsorbed state with the surface -OH group. The low adsorption energy of the interaction suggested that the adsorption is not chemical but rather a weak molecular interaction[54]. The low temperature couldn't supply enough energy for complete reaction between -OH and adsorbed DEZ. The lower energy peak between channel 230 to 275 shows that hydrogen is also trapped near the interface between the Si substrate and the growing ZnO film. It is speculated that un-reacted -OH left on the Si surface during the surface preparation remains and/or grows during the initial H_2O pulses of the ALD process. The low deposition temperature and the absence of post-annealing strongly limit hydrogen diffusion which is consistent with the heterogeneous distribution in the depth profile of ZnO films.

Fig.5a shows the hydrogen concentration depth distribution. In all cases, there is a region about 10nm thick at the surface that is richer in hydrogen than deeper into the sample. This is not due to external contamination, as will be seen below, and may be related to roughness of the film surface. Outside the ALD window, the films are thinner and so the hydrogen concentration is dominated by that of the surface region, and the depth resolution of the ERDA method is hardly sufficient to

distinguish the surface and subsurface regions. Within the ALD window the films are thick enough that we can reliably distinguish between the surface and bulk regions for hydrogen content, however a detailed examination of the hydrogen depth profiles is beyond the scope of the present work. Let us consider, then, the total hydrogen contents of the films. In the films deposited at 140℃ and 150℃ the hydrogen concentration of 7.8 at% corresponds to the introduction of about 1.2×1015 hydrogen atoms/cm2 per cycle, which is nearly twice that observed at lower temperature (100℃), suggesting that more hydrogen atoms originating from the organic fragments have been left in the film with the increase of growth rate. Although the growth rate of film deposited at 160 ℃ is nearly the same as that of films deposited at 150℃, the hydrogen concentration decreases significantly, with about 34×10^{15} atoms/cm^2, corresponding to about 5.8 atom% (As shown in Fig.S2c and S3c).

Fig.4c and 5c show the hydrogen content in ZnO films deposited at 175℃, which is smaller even than that at the lower range of the ALD window (150℃). Further increasing the deposition temperature to 300℃, the hydrogen concentration of the ZnO films decreases to its lowest value of about 6 at% (as shown in Fig.4d and 5d). This could be due to a decrease in the -OH concentration on the ZnO surface at higher temperature[38] but is also consistent with the observation of reduced carbon contamination, which if due to the incorporation of decomposed DEZ organic fragments could also lead to a reduction of hydrogen concentration. The ERDA results for other films are given in Fig.S3b and Fig.S4b. In conclusion, the hydrogen concentration in the films decreases as the deposition temperature increases, however it is not possible to know whether the hydrogen originates from residual hydroxyl groups or from DEZ decomposition products, the concentration of both of which are expected to decrease with increasing film growth temperature above the ALD window.

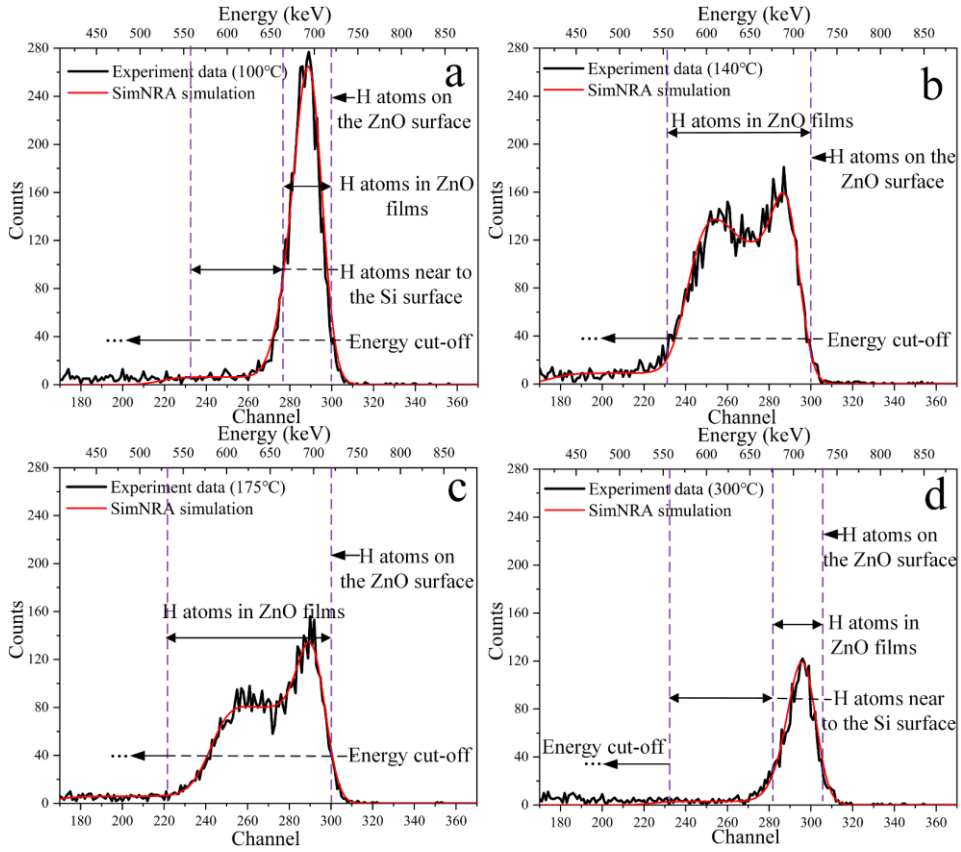

Fig.4. The ERDA spectra obtained from ZnO films as a function of the deposition temperature for 100°C (a), 150°C (b), 175°C (c) and 300°C (d), for 40 ALD cycles.

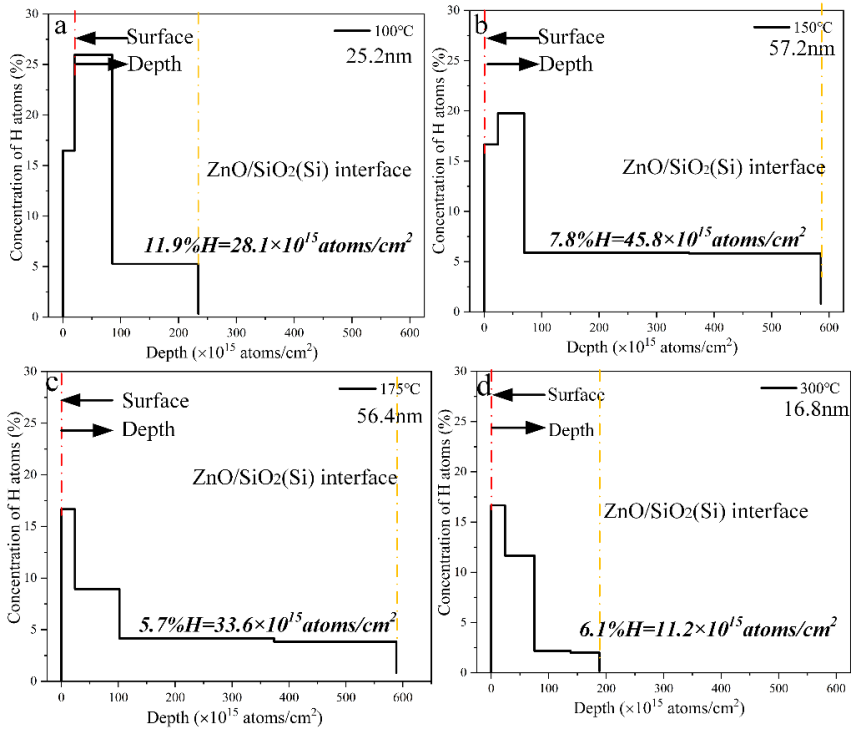

Fig.5. The hydrogen concentration depth distributions deduced from ERDA in ZnO film as a function of the deposition temperature at 100°C (a), 150°C (b), 175°C (c) and 300°C (d).

However, the dramatic decrease in the C concentration at 140°C and 150°C (Fig. 3) is not matched by a corresponding dramatic reduction of the hydrogen concentration. Ren reported that neighboring hydroxyl could facilitate the H_2O half-reaction, with the reaction of H_2O with -O-Zn-C_2H_5 preferred over reaction with -OH on the surface[21]. Moreover, the growth rate is very much higher compared to other deposition temperatures. If the hydrogen is coming initially from DEZ fragments, then the fact that a significant concentration of hydrogen remains in the film suggests to us that the hydrogen atoms from the H_2O or DEZ fragments could diffuse into the films in the ALD window. In order to determine whether the hydrogen is coming from the H_2O or DEZ fragments, we used D_2O (99.8%) as the water precursor. Since ERDA can separate these two isotopes of hydrogen, this allows us to distinguish hydrogen coming from the water vapour (deuterium) from that originating in the DEZ (hydrogen) in the ERDA spectra.

Fig.6a shows ERDA spectra obtained from 100°C, 150°C and 300 °C and the corresponding SimNRA simulations. At 100°C, the deuterium concentration is only about 17% of the total hydrogen concentration, indicating that only about 17% of hydrogen in the film originates from the labelled water (deuterium), the remaining 83% coming from DEZ fragments during the ALD process. At 150°C, only about 8% of the total film hydrogen comes from the water vapour, this ratio being even lower in the film bulk. Hence, we may suppose that most of the -OH groups produced during the water ALD cycle can almost completely react within the ALD window, and the higher content of hydrogen comes from the DEZ precursor. Previous study shows that DEZ might be dissociated into Zinc, ethyl and its fragments and so on, its ethyl groups could undergo further reaction to form ethene, ethane and butane in the reactor[50, 55]. Hence, we supposed that the redundant hydrogen will diffuse into the films, causing higher hydrogen content in the films. At 300°C the film has a lower overall hydrogen content of about 5.4 atom%. However, the percentage of deuterium in the film is greater than 22%, illustrating a prevalence of diffusion phenomena over the desorption of fragments.

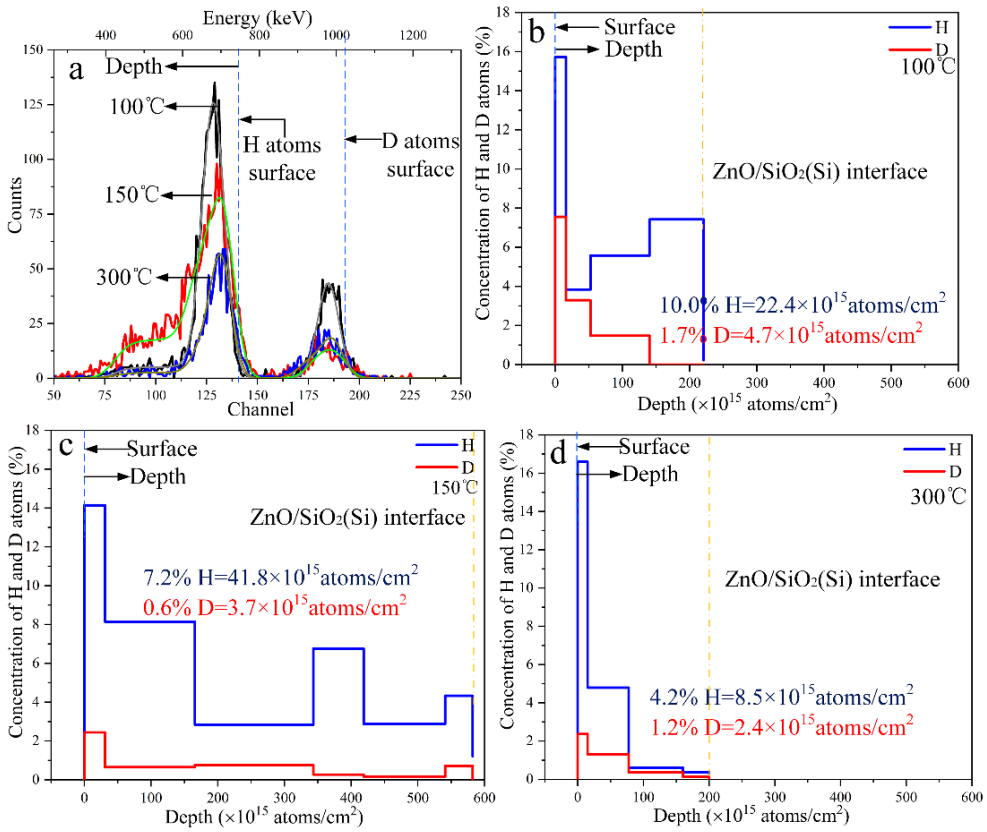

Fig.6. a: Typical ERDA spectra of ZnO films deposited at 100°C, 150°C and 300°C, (40 cycles). The hydrogen concentration depth distributions deduced from ERDA in ZnO film as a function of the deposition temperature for 100°C (b), 150°C (c) and 300°C (d).

Fig.7 shows ERDA spectra for films produced with different purge times between the precursor pulses. Fig.7a shows that the film contains about 29.3×10^{15} atoms/cm^2 of hydrogen, corresponding to about 5.1 at%, and about 4.0×10^{15} atoms/cm^2 of D - much less than the H. From Fig. 7b we observe that the total H content of the film decreases when the purge time after the water pulse is increased. However, the total film thickness also decreases, and the H concentration in the film is in fact unchanged by the increased purge time. We suggest that film growth rate decreases due to the desorption of water molecules during the purge time, leading to a reduction of the density of reactive surface sites. We propose that as -OD displaces -C_2H_5, H atoms from DEZ molecules or to a lessor extent D atoms diffuse into the structure, so that the H(D) concentration does not depend on film thickness, but only on the -OD and -C_2H_5 reaction process. Fig.7c shows the film deposited with a long purge time (60s) after the DEZ pulse, illustrating a similar trend with long H_2O purge time (60s). After the ligand exchange between -Zn-C_2H_5 and -OD, the long purge time can be used effectively to remove unreacted DEZ and C_2H_5D. In this case, the long purge time could also increase the desorption of DEZ molecules, leading again to a slightly lower growth rate compared to that obtained with the short purge times of water (30s) and DEZ (30s). The long purge time after the DEZ pulse has less influence on the film growth rate than the long water purge time. Fig.7d

shows long purge time for both half-reactions. The total H and D areal densities decrease to their lowest values of 13.4×10^{15} and 2.8×10^{15} atoms/cm^2, respectively. However, the growth rate of film is also the lowest of these four samples due to the double effect of the reduction of reactive site density and the desorption of DEZ. Fig.S4 and Fig.S5 present the films deposited with50ms and 15ms H_2O pulses, 15ms DEZ pulse, but different purge time for water half-reaction and DEZ half-reaction. The results present the same trend as that in Fig.7. Comparing Figs.7a, S4a and S5a, we can clearly see that the purge time has little effect on the H and D concentrations. Table 2 summarizes the H, D and C contents in ZnO films as a function of purge time, the C content in ZnO film is also higher than the film deposited with 100ms and 50ms water pulses. Thus, short water pulse time (15ms) means a smaller quantity of -OH groups are formed during the water half-reaction. In other words, it's not conducive to removing the ethyl groups from Zn-C_2H_5.

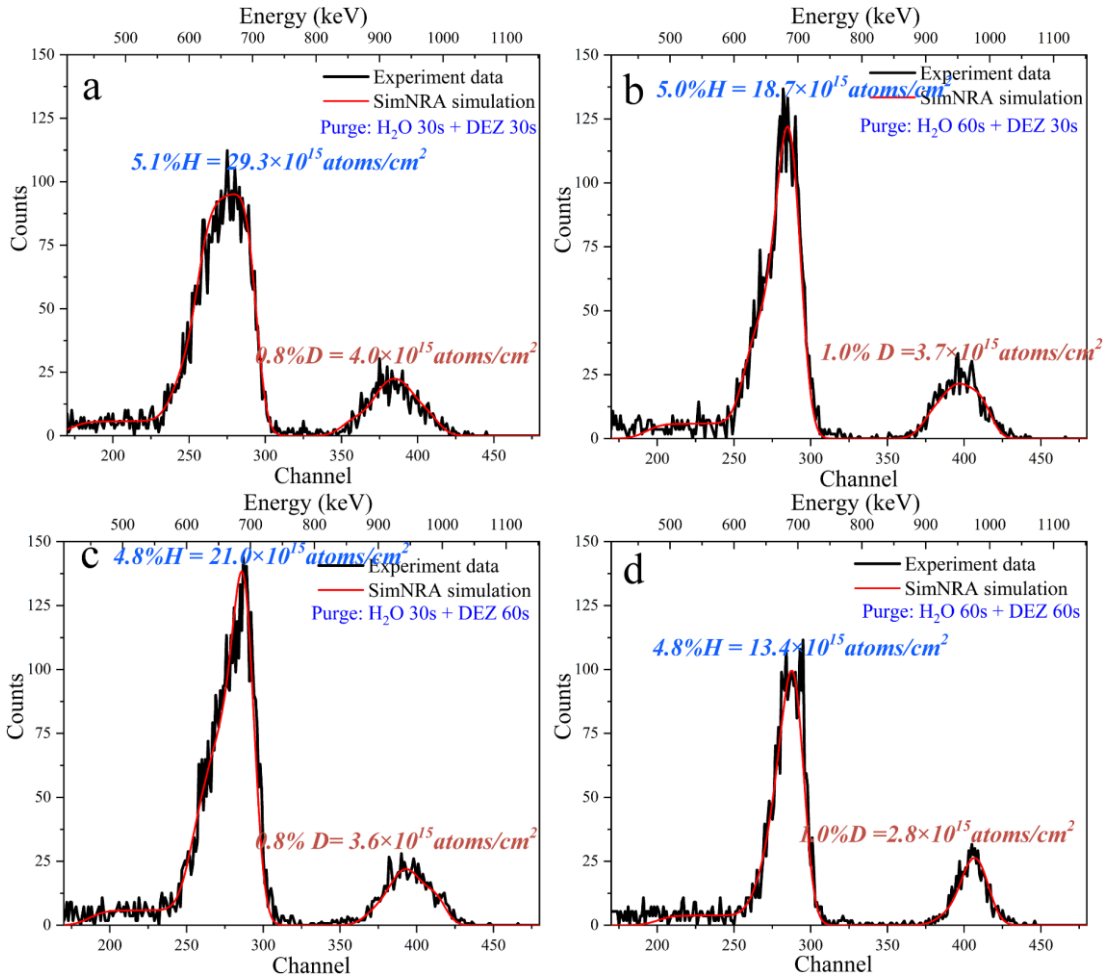

Fig.7. ERDA spectra of ZnO films deposited with different purge time; a: H_2O 30s +DEZ 30s, b: H_2O 60s +DEZ 30s, c: H_2O 30s +DEZ 60s, d: H_2O 60s +DEZ 60s. The deposition temperature was kept at 160°C, pulse time of H_2O and DEZ were 100ms and 15ms, respectively.

Table 2. The H, D and C content in the films deposited as function of purge time, the deposition temperature was kept as 160℃, the ALD cycles were 40 cycles.

Pulse time (ms)	Purge time(s)		Zn	O	H	D	C	Zn/O	H (%)	D (%)	C (%)
	H_2O	DEZ	$\times 10^{15}$ atoms/cm^2								
H_2O: 100 DEZ: 15	30	30	239.9	240.3	29.3	4.0	4.5	1.00	5.1	0.8	0.9
	60	30	169.1	177.6	18.7	3.7	7.1	0.95	5.0	1.0	1.9
	30	60	201.8	203.1	21.0	3.6	7.5	0.99	4.8	0.8	1.7
	60	60	126.8	131.4	13.4	2.8	2.8	0.96	4.8	1.0	1.0
H_2O: 50 DEZ: 15	30	30	177.6	183.6	19.2	2.9	3.7	0.97	5.0	0.8	1.0
	60	30	134.0	140.0	10.2	3.0	6.4	0.96	3.5	1.0	2.2
	30	60	165.9	171.2	12.6	3.2	6.0	0.97	3.5	0.9	1.7
	60	60	88.6	93.8	8.1	2.2	2.6	0.95	4.1	1.1	1.3
H_2O: 15 DEZ: 15	30	30	66.2	66.2	12.1	1.6	3.1	1.00	8.1	1.1	2.1
	60	30	49.0	60.9	10.5	1.3	3.6	0.81	8.4	1.0	2.9
	30	60	55.1	71.5	10.8	1.3	5.1	0.76	7.5	0.9	3.6
	60	60	36.7	44.2	6.7	1.2	2.5	0.83	7.3	1.3	2.7

The ERDA results reveal that the D concentration in the film deposited within the ALD window is lower than that of films deposited either side of the ALD window. This indicates that the -OH groups react more readily with DEZ molecules in the ALD window. From the ERDA analysis for ZnO films, we supposed that lower deposition temperature will increase the hydrogen in the films even within the ALD window. Although the highest growth rate occurs within the ALD window, the film composition is different even for the small variations of deposition temperature.

3.4 The Zn to O atomic ratio and film density

To further investigate the growth mechanism, the atomic ratio of Zn to O and layer density are presented in Fig.8 as a function of deposition temperature. The atomic ratio of Zn to O is close to 1 corresponding to stoichiometric ZnO (as shown in Fig.8a). However, although the uncertainties are quite high, there is a hint that Zn/O is higher either side of the ALD window, and then decreases again at even higher temperatures. These seem to be the same temperature regions as was observed for carbon.

Fig.8b summarizes the film density ρ deduced from atomic areal densities [Zn], [O], [C] and [H] and physical thickness h obtained respectively from RBS, NRA, and ERDA spectra and from ellipsometry, using the expression:

$$\rho = [Zn] \frac{M_{ZnO_xC_yH_z}}{N_A} \frac{1}{h}$$

$$M_{ZnO_xC_yH_z} = M_{Zn} + M_O \frac{[O]}{[Zn]} + Mc \frac{[C]}{[Zn]} + M_H \frac{[H]}{[Zn]}$$

where N_A is Avogadro's constant and $M_{ZnOxCyHz}$ is the molar mass of $ZnO_xC_yH_z$. Within the ALD window, the film density of 5.61 g/cm^3 is close to that for bulk ZnO, and increases slightly with increasing deposition temperature above the ALD window. Below the ALD window the film density decreases dramatically. This result is similar to that of [37] where a density of about 3.5 g/cm^3 was also found for ZnO films grown at 100°C. This is also consistent with the view that DEZ molecules pre-adsorbed on the Si (100) surface via a weak molecular interaction include fragments of ethyl and -Zn-C_2H_5 bonded with Si-OH leading to higher carbon and hydrogen contents in the film, responsible for the lower density of the films. As the growth temperature is increased, the ZnO films become denser because of decreasing impurity content. At temperatures above the ALD window, the density of ZnO film approaches that of bulk ZnO (5.61 g/cm^3).

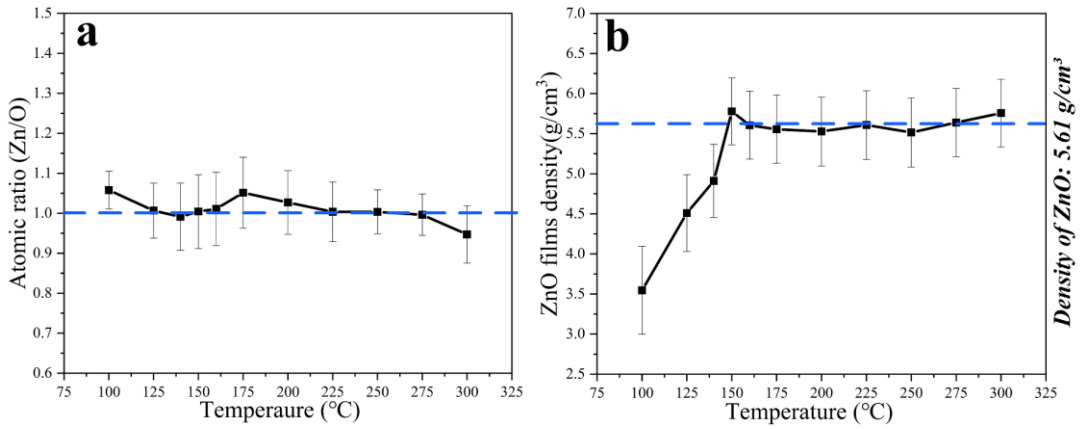

Fig.8. a: the atomic ratio of Zn to O as a function of the substrate surface temperature. b: The variation in ZnO film density as a function of the substrate surface temperature. The dashed line represents the standard bulk density.

3.5. Preferential growth of ZnO films

ZnO film grown at temperatures higher than 150°C are close to the bulk density of crystalline ZnO, and so the crystalline structure of the films was investigated by X-ray diffraction, using θ/2θ scans in a wide angular range from 20° to 60°.

Fig.9 shows the X-ray diffraction patterns of ZnO films deposited at temperatures ranging from 100-300°C. The diffraction patterns of the films grown below 125°C show no obvious peak, indicating practically no discernible long range order. The XRD pattern for the film grown at 150°C matches a polycrystalline hexagonal wurtzite ZnO structure, with three dominant peaks identified, (10.0),

(00.2) and (10.1) planes (PDF#36-1451) and a dominant crystal orientation of (10.1). As the growth temperature is increased to 175℃ and then 200℃, the films continue to show (10.0), (00.2) and (10.1) peaks in the XRD spectrum, however, the dominant orientation shifts to (00.2). This shows that the orientation of ZnO films changes from polycrystalline to a preferential out-of-plane texture. For deposition temperatures higher than 200℃, the orientation corresponding to (10.0) and (10.1) has disappeared, indicating that the orientation of (00.2) has completely dominated. According to the XRD patterns at different deposition temperatures, we can distinguish three preferential growth directions in three different temperature zones. Zone 0: 100-150℃, Zone 1: 150-200℃, Zone 2: 200-300℃.

In Zone 0, we suggest that the high carbon contamination in the films, together with the low growth temperature reduces atomic mobility and impedes the relaxation necessary for crystalline growth, leading to the almost featureless XRD pattern. Near 150° where the carbon contamination is the smallest, the films grow in a polycrystalline hexagonal wurtzite structure with little evidence of texturing. ZnO crystals are known [56, 57] to grow rapidly in the [0001] direction, and such growth on the (00.2) plane, which has the lowest surface energy according to the calculation of Fujimura[12][23], could increase the film growth rate.

However, the observation of (00.2) plane alone is not a guarantee that the growth rate will be higher. The decomposition of DEZ that occurs for deposition temperatures higher than 177℃[2], results in the increase of desorption of dissociation groups. For deposition temperatures between 200 and 250℃ (zone 2), the carbon content in the film clearly increases, and we proposed that DEZ decomposition products like CH_3-CH_2- or CH_3-, could in fact inhibit Zn atom incorporation. Deposition temperatures higher than 250℃ cause a violent pre-decomposition of DEZ molecules that could reduce the growth rate. The higher growth rate at 150℃ could be due to the low surface energy of the positively charged Zn-terminated surface at the (00.2) plane. At the higher temperatures, the ZnO could be terminated by negatively charged oxygen ions which can reduce the growth rate[58]. Thus, it is quite plausible to obtain ZnO films with a single (00.2)peak and low growth rate.

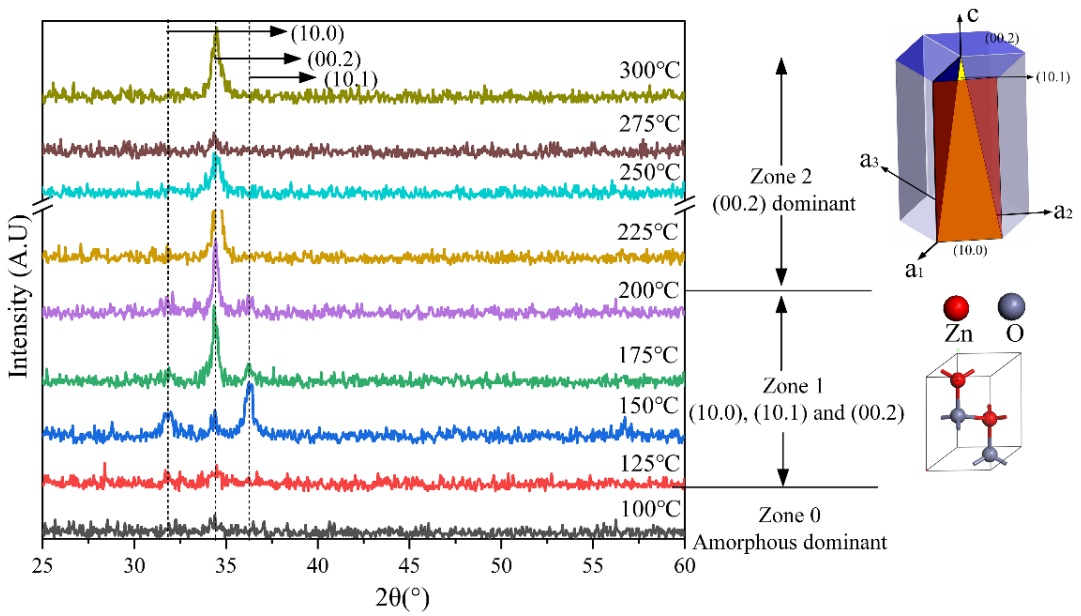

Fig.9. The XRD spectra of ZnO films deposited at different temperature.

3.6. The surface structure of ZnO films

The evolution of surface structure with deposition temperature was investigated by atomic force microscopy (AFM). Previous studies only presented ZnO surface structure dependance on growth temperature[23, 29] and we are aware of no work in which the dependance of surface structure on film thickness was investigated. Fig.10 and Fig.S6 show AFM images of ZnO obtained from samples deposited at temperatures ranging from 100-300°C, with the number of ALD cycles adjusted to obtain samples of very similar thicknesses, indicated on the AFM images.

Fig.10a shows the AFM image of ZnO films deposited at 100°C. Long wedge-shaped structures of width and length about 70nm and 700nm, respectively are observed, with the a-axis directions parallel to the substrate. Increasing the temperature to 150 or 175°C, the XRD result shows clearly that (00.2) c-axis preferred orientation appears, and the length of wedge-shaped structures became shorter. Overall, the surface structure becomes finer with increasing the deposition temperature, we proposed that the atomic arrangement changes during the ALD process. For example, Zinc terminal growth could get thicker and rougher nanostructures as compared with oxygen terminal growth in the ZnO films. Commonly, the ZnO films grown with oxygen termination prefer to grow along the junction between $(000\bar{1})$ and $(01\bar{1}0)$ rather than (00.2) surface, leading to a smaller and thiner structure. Thus, the surface structure becomes smaller with increasing deposition temperature. The wedge-shaped structures have become shorter even for films of practically the same thickness. Fig.11 and Fig.S7 show line height profiles derived from AFM pictures. The surface roughness (Rq) of the films decreases with increasing deposition temperature. The surface roughness within the ALD window is about 5nm, and higher growth temperature reduces the surface roughness, probably due to oxygen terminal growth in the ZnO films.

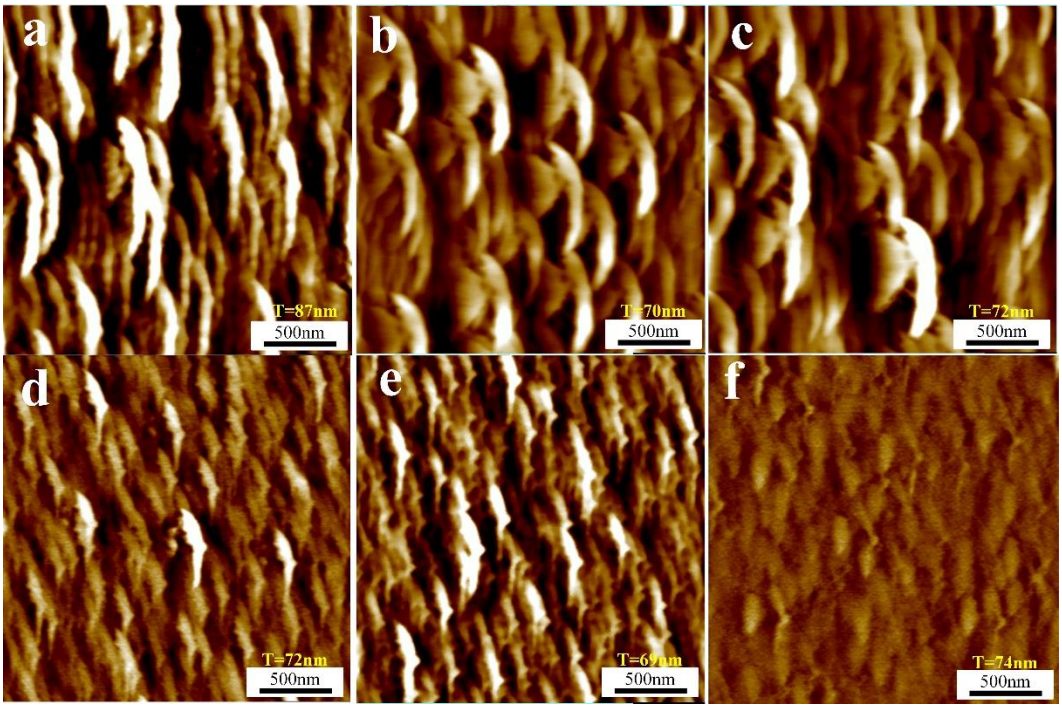

Fig.10. The AFM pictures of ZnO films deposited at different temperature, a: 100℃; b: 150℃; c: 175℃; d: 225℃; e: 275℃; f: 300℃.

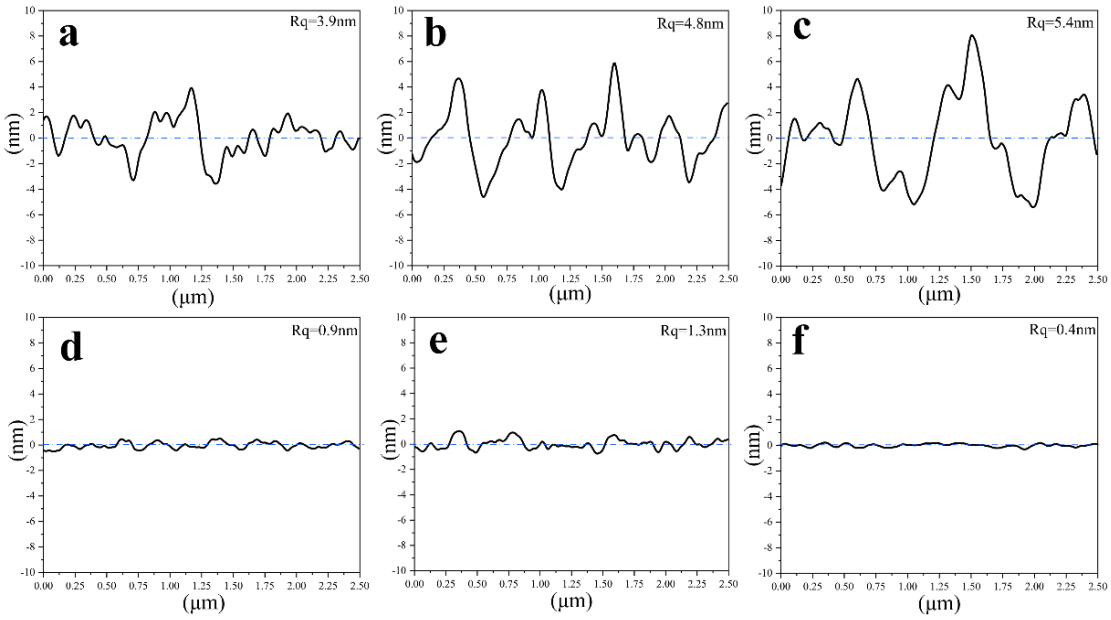

Fig.11. Cross-sectional profiles along a reference line derived from AFM pictures, a: 100℃; b: 150℃; c: 175℃; d: 225℃; e: 275℃; f: 300℃.

Conclusion

Our results show that substrate temperature significantly affects the growth rate of ZnO films grown by ALD. We revealed that the C content in the films deposited at different deposition temperatures, is lowest within the ALD window. The ZnO film densities increase with deposition temperature,

reaching the standard ZnO bulk density at 150°C and above. The C contamination in the films varies with the growth temperature even within the ALD window, reaching its lowest value of about 1 atom % at 160°C. ERDA shows that the hydrogen concentration reduces with increasing deposition temperature. Through isotope labelling (D_2O) in the process, ERDA spectra show that the deuterium concentration is less than 2 atom %, indicating that the vast majority of -OH groups on the surface are probably consumed by DEZ in the ALD window. Hydrogen atomic concentration is 4 to 12 times higher than the deuterium concentration indicating that the majority of the hydrogen in the films originates from the DEZ precursor decomposition products rather than water. In conclusion, based on the lower C and H concentrations, the film density very close to the bulk ZnO density, the Zn/O ratio of practically 1, and the maximum growth rate per cycle (GPC), we recommend a narrow ALD window with deposition temperature between 150 ℃ and 175 ℃ in order to obtain optimal ALD ZnO film growth.

Acknowledgement

The ALD system is funded in part by the CEMIP (Centre de Microélectronique de Paris Ile-de-France). The work has also benefitted from the support of the SAFIR platform of Sorbonne Université, and dedicated internal funding from the Institut des NanoSciences de Paris. We also acknowledge useful discussions with members of the French ALD network RAFALD. B. Xia is funded by the China Scholarship Council (CSC) for his PhD studies (Grant ID: 201806420022).

References

[1] A. Ashrafi, A. Ueta, H. Kumano, I. Suemune, Role of ZnS buffer layers in growth of zincblende ZnO on GaAs substrates by metalorganic molecular-beam epitaxy, Journal of crystal growth 221(1-4) (2000) 435-439.
[2] D.-Y. Son, J.-H. Im, H.-S. Kim, N.-G. Park, 11% efficient perovskite solar cell based on ZnO nanorods: an effective charge collection system, The Journal of Physical Chemistry C 118(30) (2014) 16567-16573.
[3] Y.-B. He, G.-R. Li, Z.-L. Wang, C.-Y. Su, Y.-X. Tong, Single-crystal ZnO nanorod/amorphous and nanoporous metal oxide shell composites: Controllable electrochemical synthesis and enhanced supercapacitor performances, Energy & Environmental Science 4(4) (2011) 1288-1292.
[4] X. Wang, F. Sun, Y. Duan, Z. Yin, W. Luo, Y. Huang, J. Chen, Highly sensitive, temperature-dependent gas sensor based on hierarchical ZnO nanorod arrays, Journal of Materials Chemistry C 3(43) (2015) 11397-11405.
[5] M. Tammenmaa, T. Koskinen, L. Hiltunen, L. Niinistö, M. Leskelä, Zinc chalcogenide thin films grown by the atomic layer epitaxy technique using zinc acetate as source material, Thin Solid Films 124(2) (1985) 125-128.
[6] K. Zhang, Y. Zhu, X. Liu, Z. Cui, K.W. Yeung, H. Pan, S. Wu, Sr/ZnO doped titania nanotube array: an effective surface system with excellent osteoinductivity and self-antibacterial activity, Materials & Design 130 (2017) 403-412.
[7] W.I. Park, Controlled synthesis and properties of ZnO nanostructures grown by metalorganic chemical vapor deposition: A review, Metals and materials international 14(6) (2008) 659.
[8] M. Willander, O. Nur, Q. Zhao, L. Yang, M. Lorenz, B. Cao, J.Z. Pérez, C. Czekalla, G. Zimmermann, M. Grundmann, Zinc oxide nanorod based photonic devices: recent progress in growth, light emitting diodes and lasers, Nanotechnology 20(33) (2009) 332001.
[9] M. Pan, W. Fenwick, M. Strassburg, N. Li, H. Kang, M. Kane, A. Asghar, S. Gupta, R. Varatharajan, J. Nause, Metal-organic chemical vapor deposition of ZnO, Journal of crystal growth 287(2) (2006) 688-693.
[10] A. Ohtomo, A. Tsukazaki, Pulsed laser deposition of thin films and superlattices based on ZnO, Semiconductor science and technology 20(4) (2005) S1.
[11] X. Fan, J. Lian, Z. Guo, H. Lu, Microstructure and photoluminescence properties of ZnO thin films grown by PLD on Si (1 1 1) substrates, Applied Surface Science 239(2) (2005) 176-181.
[12] M. Koleva, N. Nedyalkov, R. Nikov, R. Nikov, G. Atanasova, D. Karashanova, V. Nuzhdin, V. Valeev, A. Rogov, A. Stepanov, Fabrication of Ag/ZnO nanostructures for SERS applications, Applied Surface Science 508 (2020) 145227.
[13] A. Barhoum, G. Van Assche, H. Rahier, M. Fleisch, S. Bals, M.-P. Delplancked, F. Leroux, D. Bahnemann, Sol-gel hot injection synthesis of ZnO nanoparticles into a porous silica matrix and reaction mechanism, Materials & design 119 (2017) 270-276.
[14] V. Mote, Y. Purushotham, B. Dole, Structural, morphological, physical and dielectric properties of Mn doped ZnO nanocrystals synthesized by sol–gel method, Materials & Design 96 (2016) 99-105.
[15] T. Tynell, H. Yamauchi, M. Karppinen, R. Okazaki, I. Terasaki, Atomic layer deposition of Al-doped ZnO thin films, Journal of Vacuum Science & Technology A: Vacuum, Surfaces, and Films 31(1) (2013) 01A109.
[16] E. Langereis, S. Heil, M. Van De Sanden, W. Kessels, In situ spectroscopic ellipsometry study on the growth of ultrathin TiN films by plasma-assisted atomic layer deposition, Journal of applied Physics 100(2) (2006) 023534.
[17] J. Ferguson, A. Weimer, S. George, Surface chemistry and infrared absorbance changes during ZnO atomic layer deposition on Zr O 2 and Ba Ti O 3 particles, Journal of Vacuum Science & Technology A: Vacuum, Surfaces, and Films 23(1) (2005) 118-125.

[18] T. Tynell, M. Karppinen, ZnO: Hydroquinone superlattice structures fabricated by atomic/molecular layer deposition, Thin Solid Films 551 (2014) 23-26.
[19] C. Besleaga, G. Stan, A. Galca, L. Ion, S. Antohe, Double layer structure of ZnO thin films deposited by RF-magnetron sputtering on glass substrate, Applied surface science 258(22) (2012) 8819-8824.
[20] R.L. Puurunen, Growth per cycle in atomic layer deposition: a theoretical model, Chemical Vapor Deposition 9(5) (2003) 249-257.
[21] J. Ren, Initial growth mechanism of atomic layer deposition of ZnO on the hydroxylated Si (1 0 0)-2× 1: A density functional theory study, Applied surface science 255(11) (2009) 5742-5745.
[22] T. Weckman, M. Shirazi, S.D. Elliott, K. Laasonen, Kinetic monte carlo study of the atomic layer deposition of zinc oxide, The Journal of Physical Chemistry C 122(47) (2018) 27044-27058.
[23] S.-Y. Pung, K.-L. Choy, X. Hou, C. Shan, Preferential growth of ZnO thin films by the atomic layer deposition technique, Nanotechnology 19(43) (2008) 435609.
[24] S. Jeon, S. Bang, S. Lee, S. Kwon, W. Jeong, H. Jeon, H.J. Chang, H.-H. Park, Structural and electrical properties of ZnO thin films deposited by atomic layer deposition at low temperatures, Journal of the Electrochemical Society 155(10) (2008) H738-H743.
[25] S.-K. Kwon, D.-W. Kim, Y.-H. Jung, B.-J. Lee, Effect of process parameters on remote PEALD for highly transparent ZnO film growth, J Korean Phys Soc 55 (2009) 999-1004.
[26] K. Tapily, D. Gu, H. Baumgart, G. Namkoong, D. Stegall, A. Elmustafa, Mechanical and structural characterization of atomic layer deposition-based ZnO films, Semiconductor science and technology 26(11) (2011) 115005.
[27] P. Poodt, R. Knaapen, A. Illiberi, F. Roozeboom, A. van Asten, Low temperature and roll-to-roll spatial atomic layer deposition for flexible electronics, Journal of Vacuum Science & Technology A: Vacuum, Surfaces, and Films 30(1) (2012) 01A142.
[28] M.B.M. Mousa, C.J. Oldham, J.S. Jur, G.N. Parsons, Effect of temperature and gas velocity on growth per cycle during Al2O3 and ZnO atomic layer deposition at atmospheric pressure, Journal of Vacuum Science & Technology A: Vacuum, Surfaces, and Films 30(1) (2012) 01A155.
[29] P. Boryło, K. Matus, K. Lukaszkowicz, J. Kubacki, K. Balin, M. Basiaga, M. Szindler, J. Mikuła, The influence of atomic layer deposition process temperature on ZnO thin film structure, Applied Surface Science 474 (2019) 177-186.
[30] A. Seweryn, R. Pietruszka, B.S. Witkowski, A. Wierzbicka, R. Jakiela, P. Sybilski, M. Godlewski, Structural and Electrical Parameters of ZnO Thin Films Grown by ALD with either Water or Ozone as Oxygen Precursors, Crystals 9(11) (2019) 554.
[31] H. Beh, D. Hiller, M. Bruns, A. Welle, H.-W. Becker, B. Berghoff, C. Sürgers, R. Merz, M. Zacharias, Quasi-metallic behavior of ZnO grown by atomic layer deposition: the role of hydrogen, Journal of applied physics 122(2) (2017) 025306.
[32] H. Makino, A. Miyake, T. Yamada, N. Yamamoto, T. Yamamoto, Influence of substrate temperature and Zn-precursors on atomic layer deposition of polycrystalline ZnO films on glass, Thin Solid Films 517(10) (2009) 3138-3142.
[33] E. Przezdziecka, E. Guziewicz, D. Jarosz, D. Snigurenko, A. Sulich, P. Sybilski, R. Jakiela, W. Paszkowicz, Influence of oxygen-rich and zinc-rich conditions on donor and acceptor states and conductivity mechanism of ZnO films grown by ALD—Experimental studies, Journal of Applied Physics 127(7) (2020) 075104.
[34] S. Sultan, O.D. Clark, T.B. Masaud, Q. Fang, R. Gunn, M. Hakim, K. Sun, P. Ashburn, H.M. Chong, Remote plasma enhanced atomic layer deposition of ZnO for thin film electronic applications, Microelectronic engineering 97 (2012) 162-165.
[35] T. Krajewski, G. Luka, P. Smertenko, A. Zakrzewski, K. Dybko, R. Jakiela, L. Wachnicki, S. Gieraltowska, B. Witkowski, M. Godlewski, Schottky junctions based on the ALD-ZnO thin films for electronic applications, Acta Phys. Pol. A 120(6) (2011) A17-A21.

[36] Y. Kawamura, M. Tani, N. Hattori, N. Miyatake, M. Horita, Y. Ishikawa, Y. Uraoka, Low-temperature-processed zinc oxide thin-film transistors fabricated by plasma-assisted atomic layer deposition, Japanese Journal of Applied Physics 51(2S) (2012) 02BF04.
[37] M. Vähä-Nissi, M. Pitkänen, E. Salo, E. Kenttä, A. Tanskanen, T. Sajavaara, M. Putkonen, J. Sievänen, A. Sneck, M. Rättö, Antibacterial and barrier properties of oriented polymer films with ZnO thin films applied with atomic layer deposition at low temperatures, Thin Solid Films 562 (2014) 331-337.
[38] S. Kim, S. Lee, S.-Y. Ham, D.-H. Ko, S. Shin, Z. Jin, Y.-S. Min, A kinetic study of ZnO atomic layer deposition: Effects of surface hydroxyl concentration and steric hindrance, Applied Surface Science 469 (2019) 804-810.
[39] S. Lim, S. Kwon, H. Kim, ZnO thin films prepared by atomic layer deposition and rf sputtering as an active layer for thin film transistor, Thin Solid Films 516(7) (2008) 1523-1528.
[40] M. Napari, M. Lahtinen, A. Veselov, J. Julin, E. Østreng, T. Sajavaara, Room-temperature plasma-enhanced atomic layer deposition of ZnO: Film growth dependence on the PEALD reactor configuration, Surface and Coatings Technology 326 (2017) 281-290.
[41] J. Malm, E. Sahramo, J. Perälä, T. Sajavaara, M. Karppinen, Low-temperature atomic layer deposition of ZnO thin films: Control of crystallinity and orientation, Thin Solid Films 519(16) (2011) 5319-5322.
[42] D. Snigurenko, R. Jakiela, E. Guziewicz, E. Przezdziecka, M. Stachowicz, K. Kopalko, A. Barcz, W. Lisowski, J. Sobczak, M. Krawczyk, XPS study of arsenic doped ZnO grown by atomic layer deposition, Journal of alloys and compounds 582 (2014) 594-597.
[43] B. Xia, J. Ganem, S. Steydli, H. Tancrez, I. Vickridge, RBS and NRA analysis for films with high growth rate prepared by atomic layer deposition, Nuclear Instruments and Methods in Physics Research Section B: Beam Interactions with Materials and Atoms 489 (2021) 20-25.
[44] J. Davies, T. Jackman, H. Eschbach, W. Dobma, U. Wätjen, D. Chivers, Calibration of the Harwell series II Bi-implanted RBS standards, Nuclear Instruments and Methods in Physics Research Section B: Beam Interactions with Materials and Atoms 15(1-6) (1986) 238-240.
[45] L. Lemelle, F. Abel, C. Cohen, F. Guyot, Study of the (010) olivine surface by Rutherford backscattering spectrometry in channeling geometry, American Mineralogist 87(2-3) (2002) 327-332.
[46] I. Volintiru, M. Creatore, M. Van De Sanden, In situ spectroscopic ellipsometry growth studies on the Al-doped ZnO films deposited by remote plasma-enhanced metalorganic chemical vapor deposition, Journal of applied physics 103(3) (2008) 033704.
[47] W. Lennard, G. Massoumi, P. Alkemade, I. Mitchell, S. Tong, Revisiting the 12C (d, p) 13C reaction cross section using condensed gas targets, Nuclear Instruments and Methods in Physics Research Section B: Beam Interactions with Materials and Atoms 61(1) (1991) 1-7.
[48] G. Amsel, J. Nadai, E. d'Artemare, D. David, E. Girard, J. Moulin, Microanalysis by the direct observation of nuclear reactions using a 2 MeV Van de Graaff, Nuclear instruments and methods 92(4) (1971) 481-498.
[49] V. Quillet, F. Abel, M. Schott, Absolute cross section measurements for H and D elastic recoil using 1 to 2.5 MeV 4He ions, and for the 12C (d, p) 13C and 16O (d, p1) 17O nuclear reactions, Nuclear Instruments and Methods in Physics Research Section B: Beam Interactions with Materials and Atoms 83(1-2) (1993) 47-61.
[50] M. Rueter, J. Vohs, The surface reactions of ethyl groups on Si (100) formed via dissociation of adsorbed diethylzinc, Surface science 262(1-2) (1992) 42-50.
[51] M. Rueter, J. Vohs, Surface reactions in the decomposition of dimethylzinc on Si (100)-2× 1, Journal of Vacuum Science & Technology A: Vacuum, Surfaces, and Films 9(6) (1991) 2916-2922.
[52] S.W. Cho, C.H. Ahn, M.G. Yun, S.H. Kim, H.K. Cho, Effects of growth temperature on performance and stability of zinc oxide thin film transistors fabricated by thermal atomic layer deposition, Thin Solid Films 562 (2014) 597-602.

[53] D. Dodder, G. Hale, N. Jarmie, J. Jett, P. Keaton Jr, R. Nisley, K. Witte, Elastic scattering of protons by helium 4: New experiments and analysis, Physical Review C 15(2) (1977) 518.
[54] T. Weckman, K. Laasonen, Atomic layer deposition of zinc oxide: diethyl zinc reactions and surface saturation from first-principles, The Journal of Physical Chemistry C 120(38) (2016) 21460-21471.
[55] H. Dumont, A. Marbeuf, J.-E. Bourée, O. Gorochov, Pyrolysis pathways and kinetics of thermal decomposition of diethylzinc and diethyltellurium studied by mass spectrometry, Journal of Materials Chemistry 3(10) (1993) 1075-1079.
[56] P.X. Gao, Z.L. Wang, Nanoarchitectures of semiconducting and piezoelectric zinc oxide, Journal of Applied Physics 97(4) (2005) 044304.
[57] W.-J. Li, E.-W. Shi, W.-Z. Zhong, Z.-W. Yin, Growth mechanism and growth habit of oxide crystals, Journal of crystal growth 203(1-2) (1999) 186-196.
[58] Z.L. Wang, X. Kong, J.-M. Zuo, Induced growth of asymmetric nanocantilever arrays on polar surfaces, Physical Review Letters 91(18) (2003) 185502.